Journal of
Materials Chemistry A

Materials for energy and sustainability

Accepted Manuscript

This article can be cited before page numbers have been issued, to do this please use: Y. Lv, Y. Wang, M. Yang, Z. Mu, S. Liu, W. Ding and M. Ding, *J. Mater. Chem. A*, 2021, DOI: 10.1039/D0TA11797H.

ROYAL SOCIETY OF CHEMISTRY

rsc.li/materials-a

View Article Online
DOI: 10.1039/D0TA11797H

COMMUNICATION

Nitrogen Reduction through Confined Electro-catalysis with Carbon Nanotube Inserted Metal Organic Frameworks†

Received 00th January 20xx,
Accepted 00th January 20xx

DOI: 10.1039/x0xx00000x

Yang Lv[a], Yiqi Wang[a], Miao Yang[a], Zhangyan Mu[a], Shengtang Liu[a], Weiping Ding[a], Mengning Ding*[a]

Carbon-based nanomaterials are widely used in electro-catalysis because of their low cost, high conductivity and stability. However, their application towards selective electrochemical reduction of nitrogen to ammonia suffers from low activity and faradaic efficiency (FE). Here, we report a confined electrocatalysis strategy for enhanced ammonia production and FE in electrochemical nitrogen reduction reaction (eNRR), by the construction of a carbon nanotubes (CNTs or NCNTs) inserted porous metal organic framework (MOF). The CNT/NCNT serves as the catalytic center and ensures an efficient pathway for electron conduction that is essential to electrocatalysis, while the general hydrophobic within the MOF enriches the local concentration of N_2 near the catalyst active sites, and more importantly suppresses hydrogen evolution reaction (HER) to facilitate the FE. Over the systematically screened MOF and carbon nanotubes, NCNT@MIL-101(Fe) demonstrates the highest activity of 607. 35 μg h^{-1} mg^{-1}_{NCNT} and CNT@MIL-101(Fe) achieves the best FE of 37.28%. The significantly improved NRR performance of CNT@MOFs and NCNT@MOFs demonstrate the successful employment of confined catalysis in the electrochemical reactions, which provides an alternative strategy for the catalyst design in nitrogen fixation.

.

Introduction

Nitrogen fixation to ammonia (NH_3) or other nitrogen containing compounds has been a most important chemical process that builds up the foundation of life and agriculture.[1,2] At present, the Haber-Bosch process is still predominantly used in industrial ammonia production, which however requires harsh conditions of high temperature (400~600 °C) and high pressure (20~40 MPa), with low NH_3 yield of 10~20% and high CO_2 emission of about 3%.[3,4] Therefore, it is urgent to find a sustainable and energy-efficient approach for alternative NH_3 production from nitrogen (N_2).[5] Substantial research efforts have been dedicated to the electrochemical nitrogen reduction reaction (eNRR) under ambient conditions, as an attractive to the energy-intensive Haber-Bosch process.[6-9] Nevertheless, the reaction rate of current eNRR approaches have been relatively low, and the destruction of nitrogen triple bond requires high over potential, at which strong hydrogen evolution reaction (HER) occurs as a competition, further reducing the faradaic efficiency (FE) of eNRR.[10] To this end, research attempts have been made to suppress HER by modulating the catalysts and electrolyte selection.[11] Integration of porous structure on/over the active site, which includes metal organic frameworks (MOFs), zeolitic imidazolate frameworks (ZIFs), covalent organic frameworks (COFs)[12-15] or other porous structures,[16-19] can significantly improve the concentration of reactive species, or facilitate the chemical conversion process through confined catalysis.[20-22] Specific for eNRR, high surface area and abundant pores from porous carbon materials provide a great number of exposed active sites and fast mass transfer for N_2 adsorption and N≡N cleavage.[23] The specific surface area of MOFs reflect the number of reaction channels, and there was a pore enrichment effect in the porous materials such as MOF, ZIF, COF and etc., where the pore structure and interior groups played a characteristic adsorption effect on small gas molecules.[24] On the other hand, successful application of specific catalyst/support interface to suppress HER demonstrates another key factor for efficient eNRR.[25] Suppressing HER is also achieved *via* porous ZIF-8 coating on the Au/Ag electrode surface, where hydrophobic ZIF-8 framework effectively limited the entry of water molecules and greatly suppressed HER, leading to a high selectivity of eNRR.[26,27] The relative hydrophobic environment can further enhance the adsorption of N_2.[28] In addition, utilization of the Le Chatelier's principle has also been demonstrated, achieving better eNRR efficiency by shifting the chemical equilibrium with low pressure.[29]

To date, most effective catalytic systems for eNRR are based on noble metals such as Au,[27] Pb,[30] and Ru,[31] while catalysts based on non-noble metals have also been reported but with relatively lower activities.[32-34] Carbon-based materials generally adsorb and activate N_2 on their structural defects or sharp texture.[35,36] In addition, electron-deficient B dopants on 2D graphene could facilitate

[a] *Key Lab of Mesoscopic Chemistry, School of Chemistry and Chemical engineering, Nanjing University, Nanjing 210023, China. Email: mding@nju.edu.cn*

†Electronic Supplementary Information (ESI) available: Experimental section, characterization, including one PDF with 28 supporting figures and 3 supporting tables. See DOI: 10.1039/x0xx00000x

View Article Online
DOI: 10.1039/D0TA11797H

chemisorption of negatively polarized N atoms and promoted N-N cleavage during eNRR.[37] Even though the FE and NH_3 yield of carbon-based materials are relatively lower than noble metal-based catalysts, it is worth exploring due to its low-cost and potential durability. To this end, if a porous and hydrophobic microenvironment is constructed over the surface of high conductivity carbon material, it can concurrently enrich N_2 thus keeping a high local nitrogen concentration around catalytic sites, prevent the entrance of H_2O molecules thereby suppressing HER, and provide efficient electron transport pathway that are necessary for the electrochemical process.

Herein, we present a combined catalytic approach that includes the synergic effects of confined electrocatalysis, selective chemical diffusion and electrical transport facilitation, using CNT or N-doped CNT inserted MOFs (CNT@MOFs and NCNT@MOFs) as a proof-of-concept demonstration (Scheme 1). In a typical CNT@MOF hybrid nanostructure, the CNT serves as the catalytic center and more importantly ensures an efficient electron conduction pathway for electrocatalysis, and the relative hydrophobic MOF ensures local N_2 enrichment, the inhibition of water entrance (thus the suppression of HER competition), and facilitation of the desorption/diffusion of NH_3 product (polar molecule). The CNT@MOFs materials can be obtained from a universal and facile hydrothermal synthesis, leading to catalyst tunability according to the controlled adsorption and hydrophobic capacity from combination of different CNTs and MOFs entities.

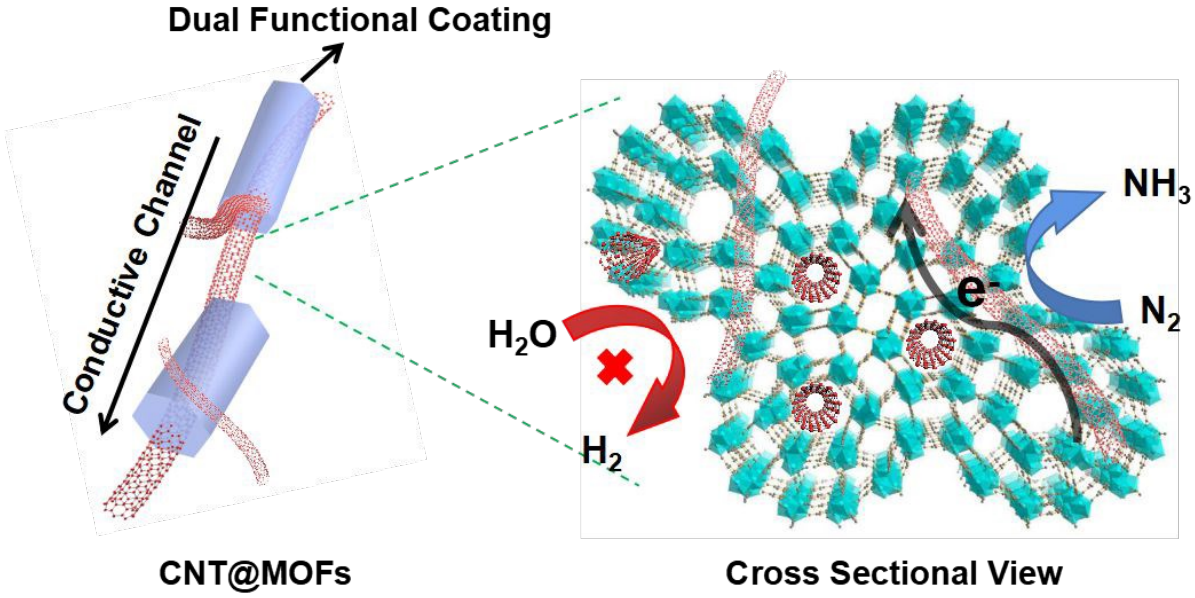

Scheme 1. Nitrogen reduction enhancement through 1) nitrogen enrichment; 2) hydrophobic HER suppression and 3) efficient conducting network of CNTs *via* carbon nanotube inserted MOFs.

Results and discussions

General preparations of CNT@MOFs and NCNT@MOFs were achieved through the one-step hydrothermal synthesis of MOFs in the presence of pre-suspended CNTs or NCNTs. The experimental details are schematically illustrated (Fig. S1†) and can also be found in Methods section.[38-41] Fig. 1a-f shows the SEM and TEM images of typical CNT@MOF structure, such as UIO-66, CNT@UIO-66 and NCNT@UIO-66, revealing that the CNTs or NCNTs were successfully inserted into corresponding MOF materials. The neighboring crystals are connected by CNTs/NCNTs to ensure the network conductivity. Other samples of CNT/NCNT inserted BIT-58, CAU-17, and MIL-101(Fe) have also be achieved (Fig. S2-S4†).

Powder XRD was carried out to determine the crystalline structure and composition of the CNT@MOFs. As shown in Fig. 1g, the XRD of CNT@MOFs and NCNT@MOFs are consistent with the corresponding MOFs crystalline structure with no other heteropeaks. In certain cases such as CNT@CAU-17 and NCNT@CAU-17, the overall crystallinity of CAU-17 is not high, which may be due to the limited crystal growth in the presence of CNTs/NCNTs. Nonetheless, introduction of CNTs/NCNTs did not alter the crystalline phase of CAU-17, therefore retain the porous characteristic and adsorption capacities of CNT@MOFs and NCNT@MOFs. Similar conclusion can also be found in CNT/NCNT@UIO-66, CNT/NCNT@BIT-58, and CNT/NCNT@MIL-101(Fe), which further indicates that this synthetic methodology can be universally applied to a broad range of CNT and MOF combinations.

BET was employed to probe the specific surface areas (SSA) of MOFs after the insertion of CNTs, which also measures the ability for nitrogen enrichment. As shown in Fig. 2a&2d, the SSA of UIO-66 is 958.3 m^2g^{-1}. Although the SSA is decreased in CNT@UIO-66 (395.8 m^2g^{-1}) and NCNT@UIO-66 (361.1 m^2g^{-1}) after hybridization, it is a significant improvement as compared to bare CNTs/NCNTs (127.6 m^2g^{-1} and 56.5 m^2g^{-1}). Similar results were also observed in BIT-58, CAU-17 and MIL-101(Fe) systems (Fig. 2b and Fig. S5 & Table S1†), which provide the general basis towards N_2 enrichment. Water contact angle is an important index to evaluate the overall

hydrophobicity of materials, which can also reflect the microenvironment within the porous MOF structure and hence the ability to suppress HER over NRR. Fig. 2e&2i. and Fig. S6† show the systematically tested water contact angles of CNT/NCNT@UIO-66, CNT/NCNT@BIT-58, CNT/NCNT@CAU-17 and CNT/NCNT@MIL-101(Fe) (34.1±0.8°/32.9±2.4°, 43.3±2.5°/48.6±3.5°, 29.3±0.3°/35.4±2.2° and 57.7±4.6°/71.7±2.8°, respectively) (Fig. 2c and Fig. S7†) are all larger than that of CNT/NCNT(22±0.4°/20.5±2.1°). Moreover, the current densities of CNT/NCNT@MOFs are much lower compared to that of CNT/NCNTs under Ar, which suggested that the HER was inhibited and the degrees of suppression are consistent with the relative hydrophobicity (Fig. 2c&2f). To verify the effect of relative hydrophobic environment on suppressed HER, the electrochemical surface areas (ECSA) were obtained by extracting the double layer capacitance (C_{dl}) from the CV measurements under Ar.[42,43] As shown in Fig. 2g&2h, the C_{dl} value of CNT/NCNT@MIL-101(Fe) are calculated to be 0.105/0.091 mF cm^{-2}, which are much compared to CNT/NCNTs (2.472/4.06 mF cm^{-2}), demonstrating the lower electrocatalytic activities of CNT/NCNT@MIL-101(Fe) for HER. In addition, the electrocatalytic activities of other CNT@MOFs for HER are basically consistent with trend of water contact angles (Fig. S7†). These results confirm that the relathydrophobic capacities of CNT/NCNT@MOFs were generally improved compared with pristine CNTs/NCNTs and pure MOFs, which serve as an important base for the inhibition of HER and improved FE for NRR. It should also be mentioned that the relative hydrophobic local environment could also presumably facilitate the desorption of NH_3 (with a dipole moment itself) and their consequent diffusion into the solution.

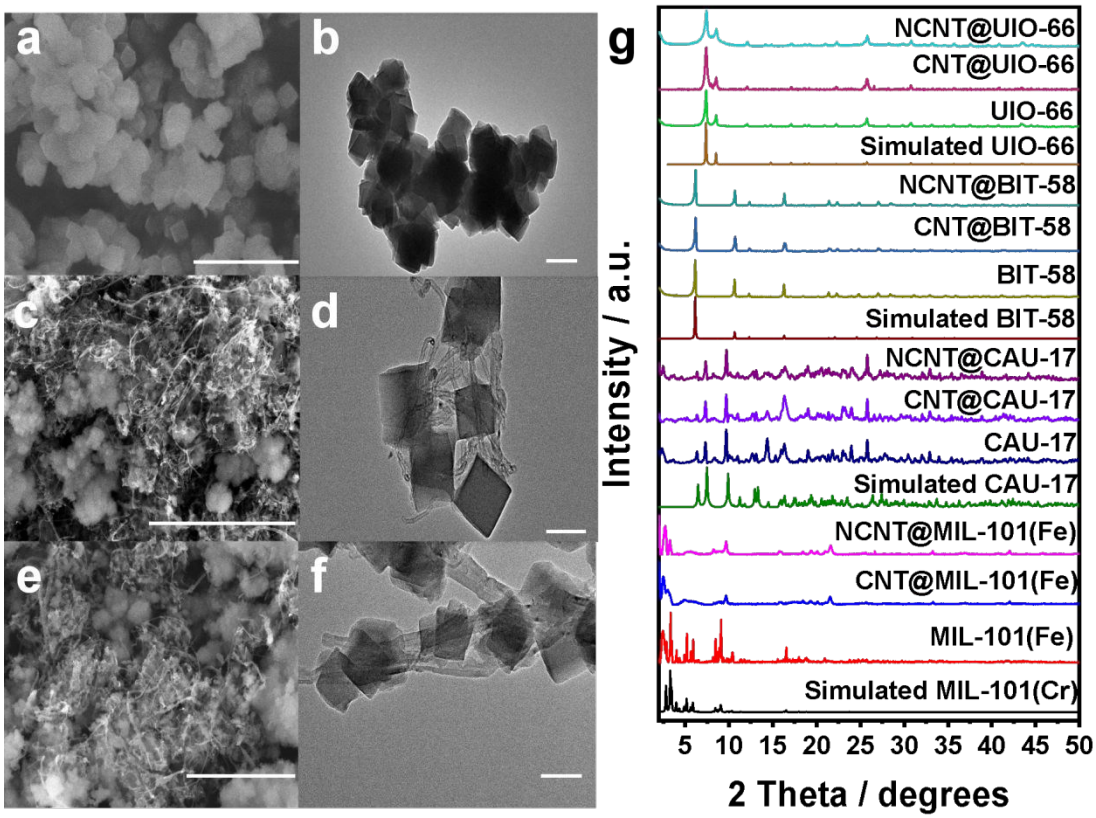

Fig. 1. Scanning Electron Microscopy (SEM) images of (a) UIO-66, (c) CNT@UIO-66, and (e) NCNT@UIO-66. Transmission Electron Microscopy (TEM) images of (b) UIO-66, (d) CNT@UIO-66, and (f) NCNT@UIO-66. (g) XRD patterns of MOF systems. Scale bars are 1 μm in (a), 200 nm in (b), 3 μm in (c) and (e), and 100 nm in (d) and (f).

To evaluate the electrocatalytic NRR activities, the as-prepared CNT/NCNT@MOFs catalysts were tested in 0.05 M H_2SO_4 with saturated high-purity N_2 (≧99.999 %), using saturated high-purity Ar (≧99.999 %) as background control. We first tested pristine CNTs and NCNTs, and obtained the highest NH_3 yield rate and FE of 1.54 μg h^{-1} mg$^{-1}_{cat.}$/3.16 μg h^{-1} mg$^{-1}_{cat.}$ and 1.77%/1.87%, respectively. As shown in Fig. 3a&3e and Fig. S10&S11†, the eNRR activity of NCNTs is slightly better than that of CNTs, probably due to the N vacancies that facilitate N_2 adsorption or the stabilization of N-H intermediates *via* hydrogen bonding.[44] The eNRR activities of all CNT/NCNT@MOF catalysts were then systematically investigated. Specifically for CNT/NCNT@CAU-17 (Fig. 3b&3f), the UV-vis absorption spectra detected by the indophenol blue method (Fig. S8†) indicate that the enhanced electrocatalytic N_2 reduction can be achieved by CNT/NCNT@CAU-17 at selected potentials.[45] As shown in Fig. 3c&3g, NH_3 yield rates of CNT/NCNT@CAU-17 reached to 11.92±0.083 μg h^{-1} mg$^{-1}_{cat.}$/13.30±0.01 μg h^{-1} mg$^{-1}_{cat.}$ at -0.45 V, with FEs of 31.27±0.29%/19.90±0.25% at -0.4 V/-0.45 V. These results are 18 and 11 times higher than that of pristine CNTs and NCNTs, and the significantly improved eNRR performance is

comparable with other state-of-the-art carbon-based electrocatalysts (Table S2†), but based on a simple strategy of confined electrocatalysis without the introduction of additional catalytic sites. Furthermore, CNT/NCNT@CAU-17 manifest considerable stabilities, with only small change in NH_3 yield and FE during consecutive recycling between N_2-saturated and Ar-saturated electrolytes for 12 hrs (Fig. 3d&3h. and Fig. S12†). Control experiments using Ar and N_2-saturated post electrolytes under -0.45 V and open circuit potential demonstrate evident accumulation of generated ammonia and ignorable accumulation of contaminated ammonia in the tests (Fig. S12†).

To further confirm the universality of the strategy, we have conducted systematic and detailed investigations on CNT/NCNT@UIO-66, CNT/NCNT@BIT-58 and CNT/NCNT@MIL-101(Fe), the best UV-Vis absorption spectra of CNT/NCNT@MOFs are demonstrated in Fig. 3j and Fig. S19†) and the results clearly show that the variety of assembled CNT/NCNT@MOFs with different combination of building blocks all possess sufficient eNRR performance (activities and FEs) with good stabilities. NH_3 yield rates of CNT/NCNT@UIO-66 reached to 3.811 μg h^{-1} $mg^{-1}_{cat.}$/6.081 μg h^{-1} $mg^{-1}_{cat.}$ at -0.55 V/-0.6 V, with FEs of 15.14%/18.13% at -0.55V, which are 8.55/9.7 times higher than that of CNT/NCNT; CNT/NCNT@BIT-58 achieved the NH_3 yield rates of 4.135 μg h^{-1} $mg^{-1}_{cat.}$/8.108 μg h^{-1} $mg^{-1}_{cat.}$ at -0.45 V, and FEs of 12.4%/15.03% at -0.45V, 7.06/8.03 times higher than that of CNT/NCNT; for CNT/NCNT@MIL-101(Fe), the NH_3 yield rates are 5.514 μg h^{-1} $mg^{-1}_{cat.}$/6.97 μg h^{-1} $mg^{-1}_{cat.}$ at -0.45 V, and FEs are 37.28%/25.15% at -0.45V, which are 21.06/13.45 times higher than that of CNT/NCNT (Fig. S13-S18†). Moreover, the NH_3 yield rates of NCNT@MOFs are in general slightly higher than those of CNT@MOFs (as shown in Fig. 3k-l and Fig. S20†), which are consistent with the data of CNT/NCNT, indicating that MOFs mainly plays the role of enriching N_2 and relative hydrophobic suppression of HER in the reaction. To verify the stabilities of the CNT@MOFs, we tested the XRD, SEM and TEM of CNT/MOFs after electrolysis of 6 cycles. As shown in Fig. S21 and S22†, the crystalline structures of all the CNT@MOFs remained, with only a little change of morphology (such as the edge smoothness), thus confirming the satisfying stability of the CNT@MOFs.

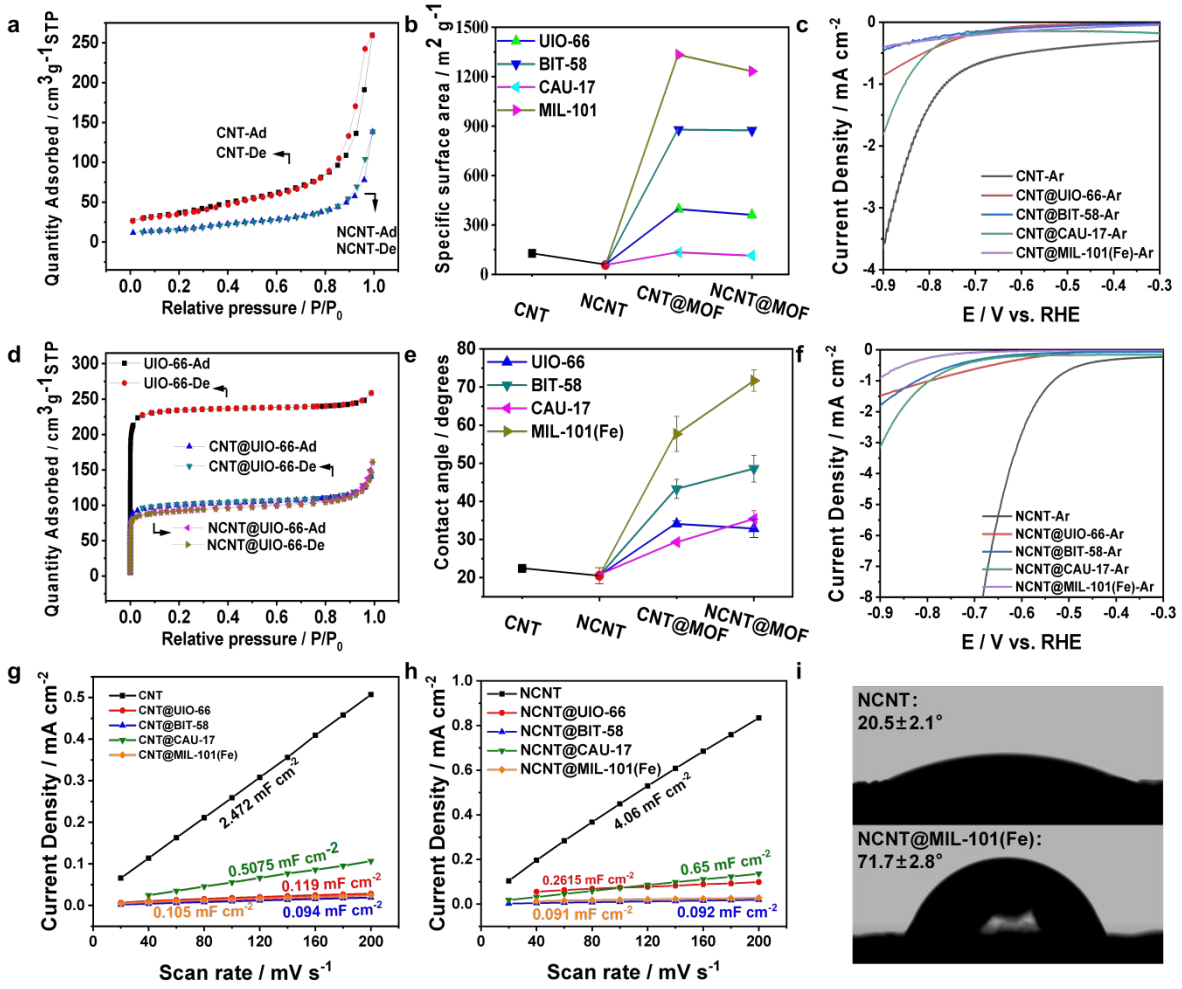

Fig. 2. (a), (d) N_2 adsorption-desorption isotherms of CNT/NCNT and UIO-66 system (as a representative MOF, for others see supporting information). (b) Specific surface areas of CNT/NCNT@MOFs. (e) Water Contact angles plot of CNT/NCNT@MOFs. (c), (f) LSV curves of CNT/NCNT and CNT/NCNT@MOFs under Ar. (g), (h) Capacitive current densities derived from CV curves against scan rates for CNT/NCNTs and CNT/NCNT@MOFs. (i) Water contact angle images of CNT/NCNT and CNT/NCNT@MIL-101(Fe) (as a representative MOF, for others see supporting information).

View Article Online
DOI: 10.1039/D0TA11797H

COMMUNICATION

In order to further clarify the rule of MOFs coating in the NRR enhancement in the CNT/NCNT@MOFs, the NRR performance of pure MOFs have been further evaluated. Date exhibited in Fig. 3i and Fig. S23-26† indicate that the pure MOFs generally have no NRR activities, except for CAU-17 (yield rate of 3.98 μg h^{-1} $mg^{-1}_{cat.}$ and FE of 11.2%), which could be a result of unsaturated CAU-17 that contributed Bi sites for additional NRR catalysis. Mechanistic aspects of eNRR over CNT/NCNT@MOFs and the role of MOFs have been investigated in detail by analyzing the BET and water contact angle results and their correlations to the electrocatalytic behaviours. Interestingly, the NH_3 yield rates from CNT/NCNT@MOFs samples were normalized to the amount of actual active carbon (i.e., the mass of CNT/NCNT), as shown in Fig. 4a&4b, we can clearly observe that the NH_3 yield rate is positively correlated with SSA and the contact angle. In particular, in Fig. 4a, we found that when the SSAs of CNT and CNT@CAU-17 were similar, CNT@CAU-17 with larger contact angle showed higher NH_3 yield rate, which also confirmed the inhibition of hydrophobicity to HER, thus promoting the eNRR; when the contact angles of NCNT and NCNT@CAU-17 were similar, NCNT@CAU-17 with larger SSA got a higher NH_3 yield rate, which proved that the positive effect of N_2 enrichment on eNRR. In general, the NH_3 yield rate is mainly determined by SSA (see Fig. S27†), while the FE is greatly affected by hydrophobicity, as shown in Fig. 4c&4d. It is worth noticing that there is an irregular eNRR

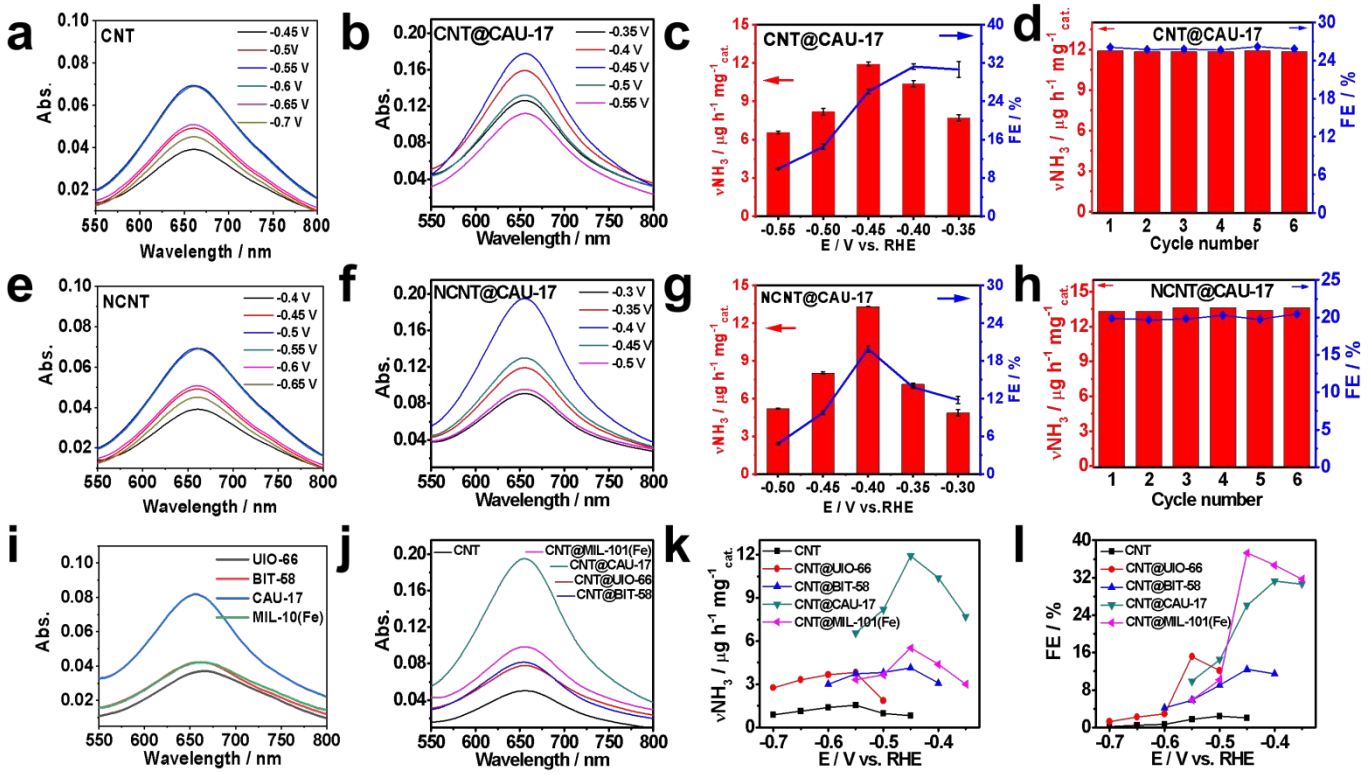

Fig. 3. (a), (e) UV-Vis absorption spectra of the electrolyte stained with indophenol blue indicator after electrolysis at selected potentials of CNT/NCNTs (b), (f) UV-Vis absorption spectra of the electrolyte stained with indophenol blue indicator after electrolysis at selected potentials of CNT/NCNT@CAU-17 (as a representative MOF, for others see supporting information). (c), (g) NH_3 yield rates and FEs of CNT/NCNT@CAU-17 at selected potentials. Error bars denote the s.d. of the yield rates and faradaic efficiency calculated from three independent samples. (d), (h) NH_3 yield rates and FEs of CNT/NCNT@CAU-17 after each cycle at -0.45 V vs. RHE. (i), (j) The highest UV-Vis absorption spectra of each pure MOFs and CNT@MOFs. (k) NH_3 yield rate of CNT@MOFs at selected potentials. (l) Corresponding FEs of CNT@MOFs.

activity of CNT/NCNT@CAU-17 which is not restricted by hydrophobicity or SSA. This is probably due to the Bi sites exposed by the unsaturated CAU-17 system, which has been identified as an excellent catalyst in the eNRR.[46-48] This assumption agrees with the unusual results of CAU-17 system in XRD, BET and contact angle. In addition, no discernible hydrazine was detected by the Watt and Chrisp method

View Article Online
DOI: 10.1039/D0TA11707H

(see Supplementary Fig. S9†) in this study (see Fig. S28-29†).[46] Overall, this obvious correlation between the eNRR performance of CNT/NCNT@MOFs with the SSA and hydrophobicity of MOF coatings confirms our strategy. In short, SSA determines the N_2 adsorption capacity of CNT/NCNT@MOFs, thus changing the local N_2 concentration on the CNT surface, while the contact angle regulates the hydrophobicity of CNT/NCNT@MOFs, resulting in different degrees of inhibition on HER, which results in a great improvement of the activity of eNRR (see Table S3†). This result also reveals the potential in the combination of our confined electrocatalysis strategy with more active sites. To further elucidate the NH_3 origin, we performed electrolysis by using $^{15}N_2$ on NCNT@CAU-17 with the maximum NH_3 yield. As shown in Fig. S30† that two peaks with a coupling constant of 72.9 Hz are detected in the baseline-subtracted ^1H NMR spectra, which is consistent with heteronuclear coupling constant between ^1H and ^{15}N of $^{15}NH^{4+}$, thus proving that all ammonia product are from N_2 gas.

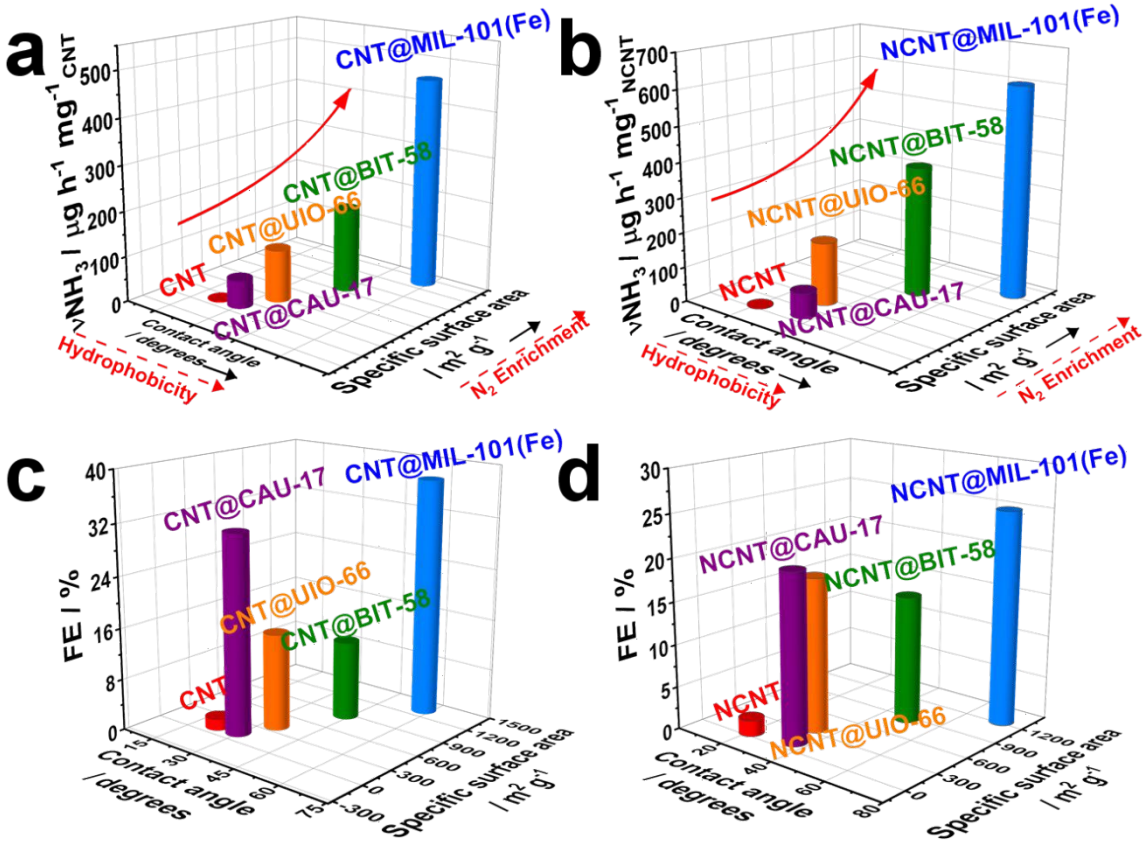

Fig. 4. (a), (b) The optimal NH_3 yield rate of CNT/NCNT@MOFs normalized to the amount of CNTs/NCNTs over different water contact angles and specific surface areas. (c), (d) The optimal FEs of CNT/NCNT@MOFs over different water contact angles and specific surface areas.

Conclusions

CNT/NCNT have been successfully inserted by a variety of MOF crystalline, resulting in a series of CNT/NCNT@MOF hybrid catalysts with significantly enhanced performance towards electrochemical nitrogen fixation. Systematic characterizations and mechanistic investigations reveal that this catalytic system benefits from the synergic combination of enrichment of nitrogen concentration, suppression of HER competition *via* hydrophobic local environment, and the facilitation of electrical transport along the CNTs network. As a result, accelerated NH_3 yield rates and improved FEs have been achieved. This strategy provides an effective and universal strategy for the design and construction of complex electrocatalytic system at mesoscopic level towards the efficient electrochemical nitrogen fixation under ambient conditions.

Authors contribution

Y. L. conceived the idea and wrote the paper. M. Y. contributed to the material characterization. Z. M. participated in the drawing of graphical abstract. S. L. and W. D. discussed the results and commented on the manuscript. M. D. projected the concept, reviewed and edited the manuscript.

Conflicts of interest

The authors have no conflicts of interest to report.

Acknowledgements

This work was financially supported by the Fundamental Research Funds for the Central Universities in China (020514380224 and 020514380195) and Natural Science Foundation of Jiangsu Province (BK20180321).

Notes and references

1 S. Y. Wang, F. Ichihara, H. Pang, H. Chen and J. H. Ye, *Adv. Funct. Mater.,* 2018, **28**, 1803309.
2 M. F. Wang, S. S. Liu, T. Qian, J. Liu, J. Q. Zhou, H. Q. Ji, J. Xiong, J. Zhong and C. L. Yan, *Nat. Commun.*, 2019, **10**, 1-8.
3 P. Mehta, F. Barboun, F. A. Herrera, J. Kim, P. Rumbach, D. B. Go, J. C. Hicks and W. F. Schneider, *Nat. Catal.*, 2018, **1**, 269-275.
4 S. L. Foster, S. I. P. Bakovic, R. D. Duda, S. Maheshwari, R. D. Milton, S. D. Minteer, M. J. Janik, J. N. Renner and L. F. Greenlee, *Nat. Catal.,* 2018, **1**, 490-500.
5 X. X. Guo, H. T. Du, F. L. Qu and J. H. Li, *J. Mater. Chem., A,* 2019, **7**, 3531-3543.
6 X. E. Liu, H. Jang, P. Li, J. Wang, Q. Qin, M. G. Kim, G. K. Li and J. Cho, *Angew. Chem. Int. Ed.,* 2019, **58**, 13329-13334.
7 P. P. Li, Z. C. Liu, T. W. Wu, Y. Zhang, L. Y. Wang, L. Wang, L. Ji, Y. Y. Zhang, Y. L. Luo, T. Wang, S. H. Liu, Y. P. Wu, M. L. Liu and X. P. Sun, *J. Mater. Chem. A,* 2019, **7**, 17761-17765.
8 X. Yang, S. Kattel, J. Nash, X. X. Chang, J. H. Lee, Y. S. Yan, J. G. G. Chen and B. J. Xu, *Angew. Chem. Int. Ed.,* 2019, **58**, 13768-13772.
9 D. Yuan, Z. X. Wei, P. Han, C. Yang, L. S. Huang, Z. X. Gu, Y. Ding, J. M. Ma and G. F. Zheng, *J. Mater. Chem. A,* 2019, **7** , 16979-16983.
10 C. Tang and S. Z. Qiao, *Chem. Sov. Rev.,* 2019, **48**, 3166-3180.
11 G. F. Chen, X. R. Gao, S. Q. Wu, X. Y. Zeng, L. X. Ding, M. Zhu and H. H. Wang, *J. Am. Chem. Soc.,* 2017, **139**, 9771-9774.
12 Q. Y. Cui, G. Q. Qin, W. H. Wang, K. R. Geethalakshmi, A. J. Du and Q. Sun, *J. Mater. Chem. A,* 2019, **7**, 14510-14518.
13 X. B. Xu, N. Farhat and X. Wang, *Chem. Mater.,* 2016, **28**, 6313-6320.
14 J. L. Liu, Y. Yang, B. Ni, H. Y. Li and X. Wang, *Small,* 2016, **13**, 1602637
15 M. Ma, X. Han, H. Q. Li, X. B. Zhang, Z. P. Zheng, L. Y. Zhou, J. Zheng, Z. X. Xie, Q. Kuang and L. S. Zheng, *Appl. Catal. B: Environ.*, 2020, **265**, 118568.
16 Z. Jin, L. Wang, E. Zuidema, K. Mondal, M. Zhang, J. Zhang, C. T. Wang, X. J. Meng, H. Q. Yang, C. Mesters and F. S. Xiao, *Science,* 2020, **367**, 193-197.
17 S. S. Zheng, Q. Li, X. G. Xue, H. Pang and Q. A Xu, *Nat. Sci. Rev.,* 2019, nwz137.
18 T. He, X. B. Xu, B. Ni, H. F. Lin, C. Z. Li, W. P. Hu and X. Wang, *Angew. Chem. Int. Ed.,* 2018, **57**, 10148-10152.
19 Z. Q. Zhang, Y. G. Chen, L. Q. Zhou, C. Chen, Z. Han, B. S. Zhang, Q. Wu, L. J. Yang, L. Y. Du, Y. F. Bu, P. Wang, X. Z. Wang, H. Yang and Z. Hu, *Nat. Commun.,* 2019, **10**, 1657-1666.
20 J. Deng, D. H. Deng and X. H. Bao, *Adv. Mater.,* 2017, **29**, 1606967.
21 D. H. Deng, X. Q. Chen, L. Yu, Wu, Q. F. Liu, Y. Liu, H. X. Yang, H. F. Tian, Y. F. Hu, P. P. Du, R. Si, J. H. Wang, X. J. Cui, H. B. Li, J. P. Xiao, T. Xu, J. Deng, F. Yang, P. N. Duchesne, P. Zhang, J. J. Zhou, L. T. Sun, J. Q. Li, X. L. Pan and X. H. Bao, *Sci. Adv.,* 2015, **1**, e1500462.
22 C. H. Turner, J. K. Johnson and K. E. Gubbins, *J. Chem. Phys.,* 2001, **114**, 1851-1859.
23 Y. M. Liu, Y. Su, X. Quan, X. F. Fan, S. Chen, H. T. Yu, H. M. Zhao, Y. B. Zhang and J. J. Zhao, *ACS Catal.,* 2018, **8**, 1186-1191.
24 W. Zhou, Q. W. Deng, G. Q. Ren, L. Sun, L. Yang, Y. M. Li, D. Zhai, Y. H. Zhou and W. Q. Deng, *Nat. Commun.*, **2020**, 11, 4481-4489.
25 H. C. Tao, C. Choi, L. X. Ding, Z. Jiang, Z. S. Han, M .W. Jia, Q. Fan, Y. N. Gao, H. H. Wang, A. W. Robertson, S. Hong, Y. S. Jung, S. Z. Liu and Z. Y. Sun, *Chem,* 2019, **5**, 204-214
26 Y. J. Yang, S. Q. Wang, H. M. Wen, T. Ye, J. Chen, C. P. Li and M. Du, *Angew. Chem. Int. Ed.,* 2019, **58**, 15362-15366.
27 H. K. Lee, C. S. L. Koh, Y. H. Lee, C. Liu, I. Y. Phang, X. M. Han, C. K. Tsung and X. Y. Ling, *Sci. Adv.,* 2018, eaar3208.
28 J. C. Zhang, B. Zhao, W. K. Liang, G. S. Zhou, Z. Q. Liang, Y. W. Wang, J. Y. Qu, Y. H. Sun and L. Jiang, *Adv. Sci.*, **2020**, 2002630.
29 H. Cheng, P. X. Cui, F. R. Wang, L. X. Ding and H. H. Wang, *Angew. Chem. Int. Ed.,* 2019, **58**, 15541-15547.
30 W. C. Xu, G. L. Fan, J. L. Chen, J. H. Li, L. Zhang, S. L. Zhu, X. C. Su, F. Y. Cheng and J. Chen, *Angew. Chem. Int. Ed.*, 2020, **59**, 3511-3516.
31 Z. G. Geng, Y. Liu, X. D. Kong, P. Li, K. Li, Z. Y. Liu, J. J. Du, M. Shu, R. Si and J. Zeng, *Adv. Mater.*, 2018, **30**, 1803498.
32 C. D. Lv, Y. M. Qian, C. S. Yan, Y. Ding, Y. Y. Liu, G. Chen and G. H. Yu, *Angew. Chem. Int. Ed.,* 2018, **57**, 10246-10250.
33 P. F. Song, H. Wang, L. Kang, B. C. Ran, H. H. Song and R. M. Wang, *Chem. Commun.,* 2019, **55**, 687-690.
34 J. X. Zhao, B. Wang, Q. Zhou, H. B. Wang, X. H. Li, H. Y. Chen, Q. Wei, D. Wu, Y. L. Luo, J. M. You, F. Gong and X. P. Sun, *Chem. Commun.,* 2019, **55**, 4997-5000.
35 W. Y. Li, T. X. Wu, S. B. Zhang, Y. Y. Liu, C. J. Zhao, G. Q. Liu, G. Z. Wang, H. M. Zhang and H. J. Zhao, *Chem. Commun.*, 2018, **54**, 11188-11191.
36 Y. Song, D. Johnson, R. Peng, D. K. Hensley, P. V. Bonnesen, L. B. Liang, J. S. Huang, F. C. Yang, F. Zhang, R. Qiao, A. P. Baddorf, T. J. Tschaplinski, N. L. Engle, M. C. Hatzell, Z. L. Wu, D. A. Cullen, H. M. Meyer III, B. G. Sumpter and A. J. Rondinone, *Sci. Adv.,* 2018, **4**, e1700336.
37 X. M. Yu, P. Han, Z. X. Wei, L. S. Huang, Z. X. Gu, S. J. Peng, J. M. Ma and G. F. Zheng, Joule, 2018, **2**, 1-13.
38 J. H. Cavka, S. Jakobsen, U. Olsbye, N. Guillou, C. Lamberti, S. Bordiga and K. P. Lillerud, *J. Am. Chem. Soc.,* 2008, **130**, 13850-13851.
39 I. A. Ken, K. Milan, J. Su, F. Mark, H. Y. Xu, X. D. Zou, O. Michael and S. Norbert, *J. Am. Chem. Soc.,* 2016, **138**, 1970-1976.
40 Y. F. Chen, S. H. Zhang, F. Chen, S. J. Cao, Y. Cai, S. Q. Li, H. W. Ma, X. J. Ma, P. F. Li, X. Q. Huang and B. Wang, *J. Mater. Chem. A,* 2018, **6**, 342-348.
41 J. Shin, M. Kim, J. Cirera, S. Chen, G. Y. Halder, T. A. Yersak, F. Paesani, S. M. Cohen and Y. S. Meng, *J. Mater. Chem. A,* 2015, **3**, 4738-4744.
42 Z. Q. Wang, Z. A. Liu, G. Du, A. M. Asiri, L. Wang, X. N. Li, H. J. Wang, X. P. Sun, L. Chen and Q. J. Zhang, *Chem. Commun.*, 2018, **54**, 810-813.
43 Z. Q. Wang, X. Ren, Y. L. Luo, L. Wang, G. W. Cui, F. Y. Xie, H. J. Wang, Y. Xie and X. P. Sun, *Nanoscale*, 2018, **10**, 12302-12307.
44 C. J. Zhao, S. B. Zhang, M. M. Han, X. Zhang, Y. Y. Liu, W. Y. Li, C. Chen, G. Z. Wang, H. M. Zhang amd H. J. Zhao, *ACS Energy Lett.,* 2019, **4**, 377-383.

View Article Online
DOI: 10.1039/D0TA11797H

45 D. Zhu, L. Zhang, R. E. Ruther and R. J. Hamers, *Nat. Mater.,* 2013, **12**, 836-841.
46 Y. C. Hao, Y. Guo, L. W. Chen, M. Shu, X. Y. Wang, T. A. Bu, W. Y. Gao, N. Zhang, X. Su, X. Feng, J. W. Zhou, B. Wang, C. W. Hu, A. X. Yin, R. Si, Y. W. Zhang and C. H. Yan, *Nat. Catal.,* 2019, **2**, 448-456.
47 R. Zhang, W. H. Kong, H. B. Wang, R. B. Zhao, H. Y. Chen, T. S. Li, B. H. Li, Y. L. Luo and X. P. Sun, *Chem. Commun.,* 2019, **55**, 5263-5266.
48 C. D. Lv, C. S. Yan, G. Chen, Y. Ding, J. X. Sun, Y. S. Zhou and G. H. Yu, *Angew. Chem. Int. Ed.,* 2018, **57**, 6073-6076.